

# High-Performance Flexible Pressure Sensor Based on Controllable Hierarchical Microstructures by Laser Scribing for Wearable Electronics

Qifeng Du, Lanlan Liu, Ruitao Tang, Jun Ai, Zhijian Wang, Qiqi Fu, Chongxiao Li, Ying Chen,\* and Xue Feng\*

Flexible pressure sensors are attracting considerable attention due to their potential applications in human health monitoring and human-machine interfaces. However, it is hard to achieve both high sensitivity and wide linear detection range, and the complicated fabrication process restricts their practical applications. Herein, a simple and scalable fabrication process for a flexible pressure sensor with high sensitivity and wide detection range has been developed by combining the silver nanowires coated, laser-ablated hierarchical microstructured polydimethylsiloxane, and an interdigital electrode. The hierarchical microstructures contribute to the high sensitivity of  $4.48 \text{ kPa}^{-1}$  and increase detection range from 0 to 65 kPa. The increase in the contact area and subsequent additional contact sites of the hierarchical microstructures lead to the high-performance. Arterial pulse, breathing, and static tremors have been measured by attaching the device to the human body. Moreover, a pressure sensor array has been fabricated to illustrate the scalability of this strategy. The results demonstrate that the flexible pressure sensor with simple and scalable fabrication capability has promising applications in wearable electronic skins.

## 1. Introduction

Flexible pressure sensors with excellent stretchability and conformability have been widely investigated due to a diversity of their applications catering to humans' future daily life, such as, electronic skins,<sup>[1,2]</sup> healthcare monitoring,<sup>[3,4]</sup> human-machine interaction,<sup>[5,6]</sup> soft robotics,<sup>[7,8]</sup> and physical rehabilitation.<sup>[9,10]</sup> In particular, flexible pressure sensors may be directly used in continuous health monitoring applications, including pulsatile flow, respiration, and human touch. Based on various transduction mechanisms, flexible pressure sensors including piezoelectricity,<sup>[11–14]</sup> capacitance,<sup>[15,16]</sup> piezoresistivity,<sup>[17–20]</sup> and triboelectricity,<sup>[21–26]</sup> have been reported. Among these pressure sensors, piezoresistive pressure sensors have been widely investigated due to their simple structure and signal processing.

In order to improve the performances of piezoresistive pressure sensors, lots of efforts have been made to develop novel materials and design various microstructures.

Recently, conductive nanomaterials, such as, graphene,<sup>[27]</sup> carbon nanotubes (CNT),<sup>[28]</sup> metal nanoparticles,<sup>[29]</sup> and nanowires<sup>[30]</sup> have been intensively used as sensing elements of flexible pressure sensors. Various microstructures, including hollow spheres,<sup>[31]</sup> micropillars,<sup>[32]</sup> microdomes,<sup>[33]</sup> micropillars,<sup>[34]</sup> bionic microstructures,<sup>[35]</sup> have been used to improve the performances of flexible pressure sensors. Shao et al. fabricated a type of high-performance and tailorable pressure sensor that merited the elastic property of conductive polypyrrole films and air gaps generated from micropillar structures. The sensitivity as high as  $1.8 \text{ kPa}^{-1}$  was achieved in the low pressure region ( $<0.35 \text{ kPa}$ ), and the limit of detection was found to be as low as  $2 \text{ Pa}$ .<sup>[36]</sup> Zhu et al. reported a flexible tactile sensor of high sensitivity based on the anisotropic pyramid microstructures of the graphene arrays. The pressure sensor had an ultrahigh sensitivity of  $5.53 \text{ kPa}^{-1}$  toward low pressure values ( $0\text{--}0.1 \text{ kPa}$ ) and an ultrafast response time of  $0.2 \text{ ms}$ .<sup>[37]</sup> Zhang et al. demonstrated a flexible and highly sensitive pressure sensor based on microdome patterned polydimethylsiloxane (PDMS) with the assistance of colloid self-assembly and replica technique. The sensor exhibited high sensitivity of  $15 \text{ kPa}^{-1}$  in the low pressure ( $<0.1 \text{ kPa}$ ) and fast response time ( $<100 \text{ ms}$ ).<sup>[38]</sup>

Dr. Q. Du, Dr. L. Liu, Dr. R. Tang, Dr. J. Ai, Dr. Z. Wang, Dr. Q. Fu, Dr. Y. Chen

Institute of Flexible Electronics Technology of THU  
Jiaxing 314000, China  
E-mail: chenying@ifet-tsinghua.org

C. Li  
Department of Electronic Engineering  
Shanghai Jiao Tong University  
Shanghai 200240, China

Dr. Y. Chen  
Qiantang Science and Technology Innovation Center  
Hangzhou 310016, China

Prof. X. Feng  
AML  
Department of Engineering Mechanics  
Tsinghua University  
Beijing 100084, China  
E-mail: fengxue@tsinghua.edu.cn

 The ORCID identification number(s) for the author(s) of this article can be found under <https://doi.org/10.1002/admt.202100122>.

© 2021 The Authors. Advanced Materials Technologies published by Wiley-VCH GmbH. This is an open access article under the terms of the Creative Commons Attribution-NonCommercial-NoDerivs License, which permits use and distribution in any medium, provided the original work is properly cited, the use is non-commercial and no modifications or adaptations are made.

DOI: 10.1002/admt.202100122

In addition, bionic microstructures also have been explored for the fabrication of high-performance piezoresistive pressure sensors. Jian et al. reported a high-performance flexible pressure sensor using carbon nanotube/graphene hybrid films as the active material and microstructured PDMS films directly molded from *epipremnum aureum* leaf. The pressure sensor exhibited a high sensitivity of  $19.8 \text{ kPa}^{-1}$  under  $0.3 \text{ kPa}$ .<sup>[39]</sup> Wang et al. reported an ultrasensitive flexible pressure sensor by combining CNT ultrathin film and micro-patterned PDMS replicated the delicate silk-based textiles. The sensing device performed a high sensitivity of  $1.8 \text{ kPa}^{-1}$  under low pressure regime ( $<0.3 \text{ kPa}$ ).<sup>[40]</sup> Su et al. proposed a bio-inspired strategy to fabricate flexible pressure sensor inspired by mimosa. In the regime of  $0\text{--}0.07 \text{ kPa}$ , a sensitivity of  $50.17 \text{ kPa}^{-1}$  was obtained and the response time to pressure changes was within  $20 \text{ ms}$ .<sup>[41]</sup>

Although significant improvements have been achieved in high sensitivity flexible pressure sensors, to achieve both high sensitivity and wide linear detection range remains a problem for their practical applications. The linear measuring range is limited by the rapid saturation of the conductive paths with the increasing pressure. Therefore, further increasing the number of conductive paths is the key to solve the contradiction between the high sensitivity and the wide linear range. Hierarchical microstructures can provide additional conductive paths with the increase of pressure, which may improve the sensitivity and measuring range of flexible pressure sensors.<sup>[42,43]</sup>

Generally, hierarchical microstructures are fabricated by traditional lithography process or mimicking the microstructures in nature, which have disadvantages of low processing efficiency and uncontrollable shape and dimensions. To solve the problems, new techniques for obtaining microstructures on flexible substrates are desired. Ultra-fast laser precision

machining can solve the above problems because it can fabricate various hierarchical microstructures with the advantages of high efficiency and large-area fabrication.<sup>[44,45]</sup>

Here we report a strategy to design and fabricate a high-performance flexible pressure sensor with printed electrodes and laser scribed hierarchical microstructures. The hierarchical microstructures are coated with silver nanowires (AgNWs) to play important roles in improving sensor performance. The fabrication process is additive, cheap, scalable and free of expensive lithography technology. The as-prepared pressure sensor exhibits a linearity range to  $22 \text{ kPa}$  with a sensitivity of  $4.48 \text{ kPa}^{-1}$ , and a linearity range from  $27$  to  $65 \text{ kPa}$  with a sensitivity of  $0.86 \text{ kPa}^{-1}$ . Moreover, the sensor presents a rapid response to pressure changes within  $7 \text{ ms}$  and excellent repeatability over  $1000$  cycles. Our flexible piezoresistive pressure sensor has been demonstrated for the detection of human physiological signals, such as wrist pulse, weak/deep breath, and imitated static tremors. Furthermore, a pressure sensor array has been exhibited for identifying the spatial pressure distribution to demonstrate the scalability of this strategy.

## 2. Results and Discussion

### 2.1. Fabrication of the Flexible Pressure Sensor

The proposed flexible pressure sensor is mainly composed of two functional layers and fabricated with microfabrication process at low price, and it can be conformally attached on human body to measure physiological parameters like pulse, respiration and motion as shown in **Figure 1a**. The fabrication as illustrated in **Figure 1b**, starts with preparing the flexible

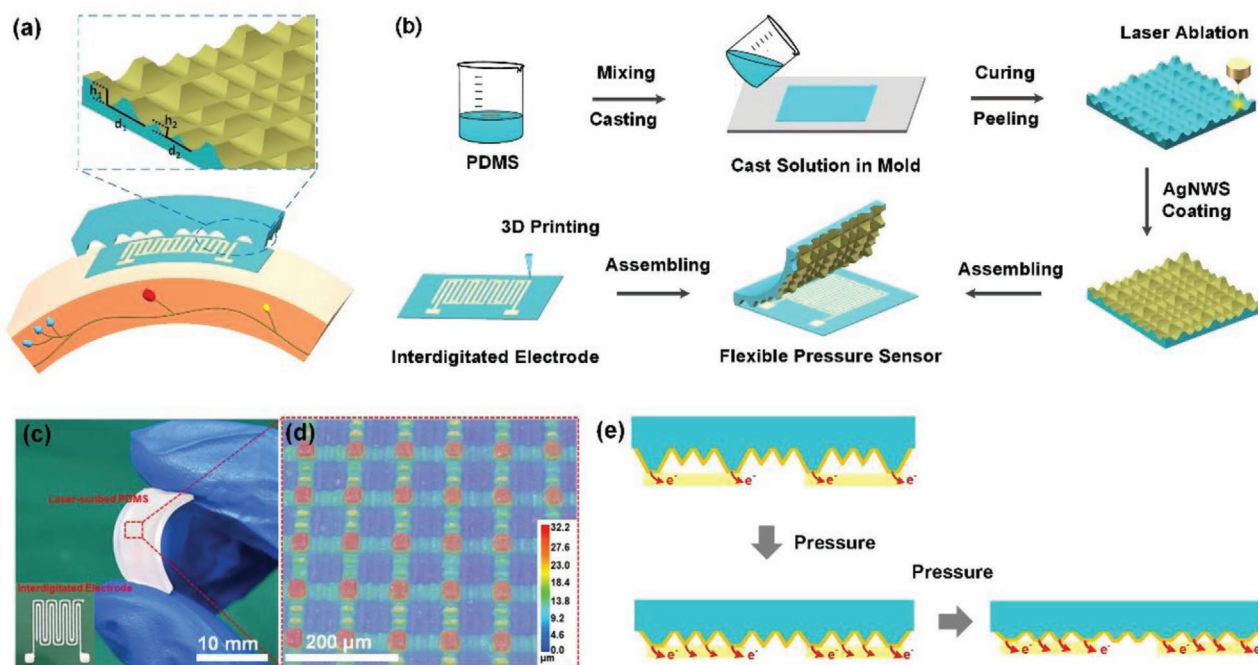


**Figure 1.** a) Schematic illustration of the flexible pressure sensor on human skin. b) The fabrication process of flexible pressure sensor. c) Digital images of laser-scribed PDMS and 3D printed interdigital electrode. d) 3D morphology of laser-scribed PDMS surface. e) The working mechanism of the pressure sensor with hierarchical microstructures.

substrate by curing the PDMS with a polymethyl methacrylate (PMMA) mold. To obtain the hierarchical microstructures, a commercial femtosecond laser with a wavelength of 355 nm is used to ablate the flat PDMS film. The light intensity distribution in the laser beam is non-uniform and the intensity at the center is stronger than that in the periphery. Thus, the hierarchical microstructures can be obtained by adjusting the laser power and the scribing pattern. Here, the first order microstructure is defined by grid line scribing, whose height is determined by the laser power. The second order microstructure is patterned by the straight line scribing, where the height is mainly dependent on the line spacing.

As shown in Figure 1c, the hierarchical microstructured PDMS is ablated by laser whose power is 1 W with a scanning speed of 800 mm s<sup>-1</sup>. The spacing of grid lines ( $d_1$ ) and filling lines ( $d_2$ ) are 40 and 20 μm, respectively. Figure 1d shows the 3D imaging of the laser scribed PDMS in which the microstructure height ( $h_1$  and  $h_2$ ) is about 30 and 20 μm, respectively. Before AgNWs deposition, the microstructured PDMS is cleaned by ethanol and treated by O<sub>2</sub> plasma to enhance the AgNWs/PDMS adhesion. The AgNWs are spin-coated as the conductive layers on the microstructured PDMS surface and dried on the hotplate at 90 °C for several minutes. The concentration of AgNWs affects the conductivity of microstructured PDMS surface and the performance of pressure sensor (Figure S1, Supporting Information). The low concentration of AgNWs results in lower sensitivity with larger  $R_b$ ; and the high concentration of AgNWs leads to lower sensitivity also with lower  $\Delta R$  (Figure S1c, Supporting Information). According to our results, the concentration of AgNWs is optimized at 10 mg mL<sup>-1</sup>, which is chosen in fabricating the flexible pressure sensor.

Different electrodes are ink-jet printed on the polyethylene glycol terephthalate (PET) film. The sensor's performance of interdigital electrode and parallel electrode are shown in Figure S2a, Supporting Information. The width of the interdigitated fingers and the spacing between two adjacent fingers are 0.2 mm. The width of the plate electrode is 1 mm and the spacing between two parallel electrodes is 8 mm. The interdigital electrode has larger contact area with AgNWs/PDMS surface compared to that of parallel electrode and shows higher sensitivity. Furthermore, different interdigitated electrodes with interdigitated finger width ( $L$ ) of 0.1, 0.2, and 0.4 mm are fabricated to evaluate the influences on sensor performance. The spacing between two adjacent interdigitated fingers is the same as the width of interdigitated finger. With increasing the width of interdigitated fingers, the conductivity of interdigitated electrode increases, resulting in increased sensitivity and decreased linear measuring range (Figure S2b, Supporting Information). Finally, the microstructured PDMS is encapsulated by the medical tape with AgNWs facing the interdigital electrode on the PET. The grid line spacing of 40 and 60 μm PDMS is named as #40 and #60 samples, respectively.

Figure 1e illustrates the sensing mechanism of the hierarchical microstructured pressure sensor. When the device is under pressure, the deformation of first order microstructures increases the contact area of the two functional layers and the resistance of the device decreases linearly. When the first order microstructures become hard to deform, the second order microstructures contact the interdigital electrode (as shown in

Figure S3, Supporting Information), and the resistance of the device decreases linearly still.

## 2.2. Characterization of the Flexible Pressure Sensor

Before characterizing the performance of the device, the theory model for fabricating hierarchical microstructures on polymer materials by laser direct writing has been analyzed. The theory model includes two modes depending on whether the adjacent lines are overlapped or not on the PDMS surface. The combined use of these two modes results in hierarchical microstructures with controlled height.

When the adjacent lines are not overlapped (Figure 2a (i)), the height ( $h_1$ ) of the microstructure can be expressed as:<sup>[46,47]</sup>

$$h_1 = \frac{2\omega f}{\alpha v} \ln U + \frac{2\omega f}{\alpha v} \ln \frac{\beta}{fmSF_{(th)}} \quad (1)$$

where  $\omega$  is the beam radius,  $\alpha$  is the absorption coefficient,  $v$  is the laser scanning speed,  $f$  is the repetition rate,  $U$  is laser power,  $m$  is the laser pulse width, and  $S$  is the beam area,  $\beta$  is the ratio of laser energy used to ablate material, and  $F_{(th)}$  is the ablation threshold fluence.

When the adjacent lines are overlapped (Figure 2a (ii)), the height ( $h_2$ ) of the microstructure can be expressed as:

$$h_2 = \frac{2fd^2}{\alpha v \omega} - \frac{2\omega f}{\alpha v} \ln \frac{\beta F_0}{F_{(th)}} \quad (2)$$

where  $d$  is the distance between the centers of adjacent spots perpendicular to the scanning direction,  $F_0$  is the fluence at the center of laser beam.

The detailed theoretical model of the laser ablating microstructures is in Supporting Information (S1). In order to study the relationship between the height of microstructures ( $h_1$ ,  $h_2$ ) and laser processing parameters ( $U$ ,  $d$ ), the other parameters are kept constant. The expressions (1) and (2) can be written as:

$$h_1 = A \ln U + B \quad (3)$$

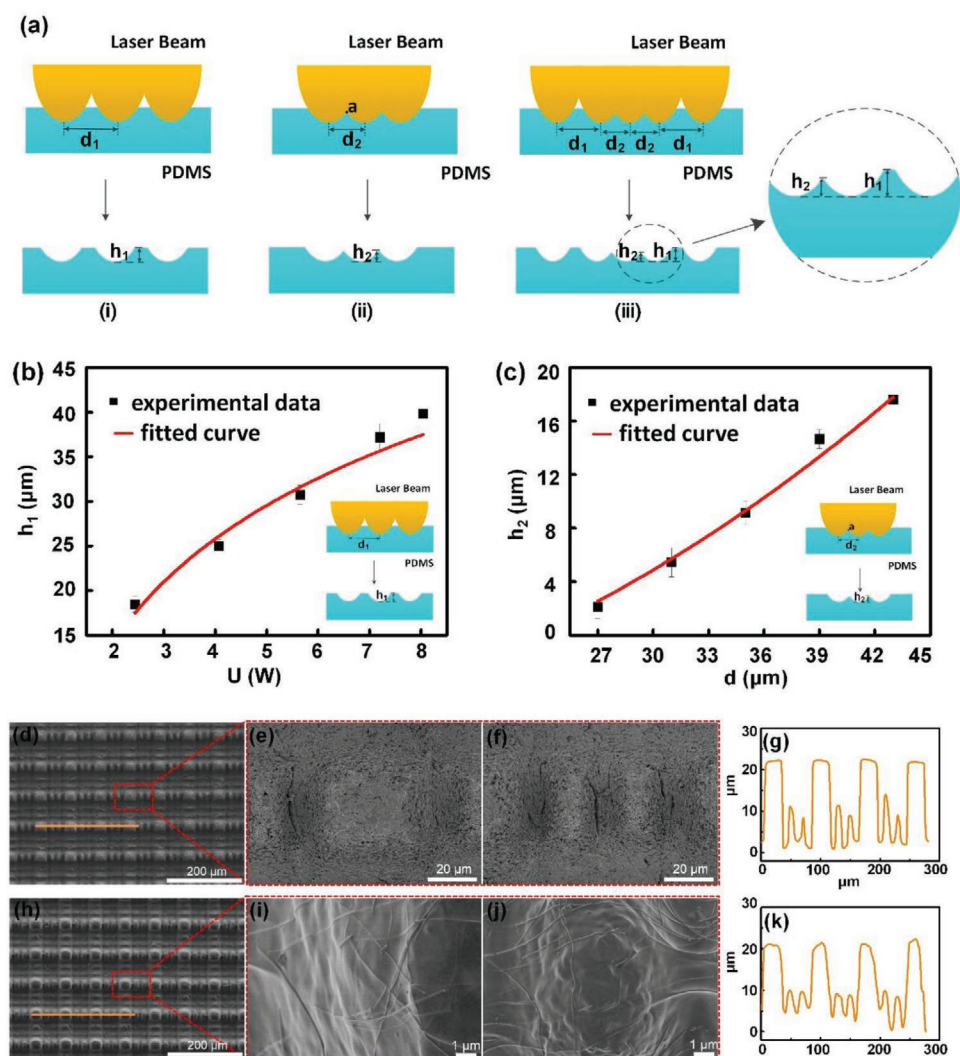
$$h_2 = Cd^2 + D \quad (4)$$

Figure 2b,c show the evolution curves of  $h_1$  and  $h_2$  along with laser power and scanning spacing, respectively. The ablation depth  $h_1$  increases with the increase of laser power, and  $h_2$  increases with the increase of distance between the centers of adjacent spots perpendicular to the scanning direction. The value of A, B, C, and D can be obtained by curve simulation.

$$A = 16.78\mu\text{m}, B = 2.51 \quad (5)$$

$$C = 0.014\mu\text{m}^{-1}, D = -7.4 \quad (6)$$

To evaluate the accuracy of the theory models, different laser parameters are employed to ablate the PDMS samples and the results of  $h_1$  and  $h_2$  are shown in Tables S1 and S2, Supporting Information. The theoretical predictive values of ablation heights are basically coincident with the experimental measurements.



**Figure 2.** a) Microstructures with different heights are achieved by adjusting laser scanning spacing. b,c) Experimental and simulated curves of microstructures with different heights at various laser powers and scanning spacings. d–f) SEM images of laser-scribed PDMS surface ( $d_1 = 40 \mu\text{m}$ ). g) Line profiles from SEM images of (d). h–j) SEM images of laser-scribed PDMS surface after coating AgNWs ( $d_1 = 40 \mu\text{m}$ ). k) Line profiles from SEM images of (h).

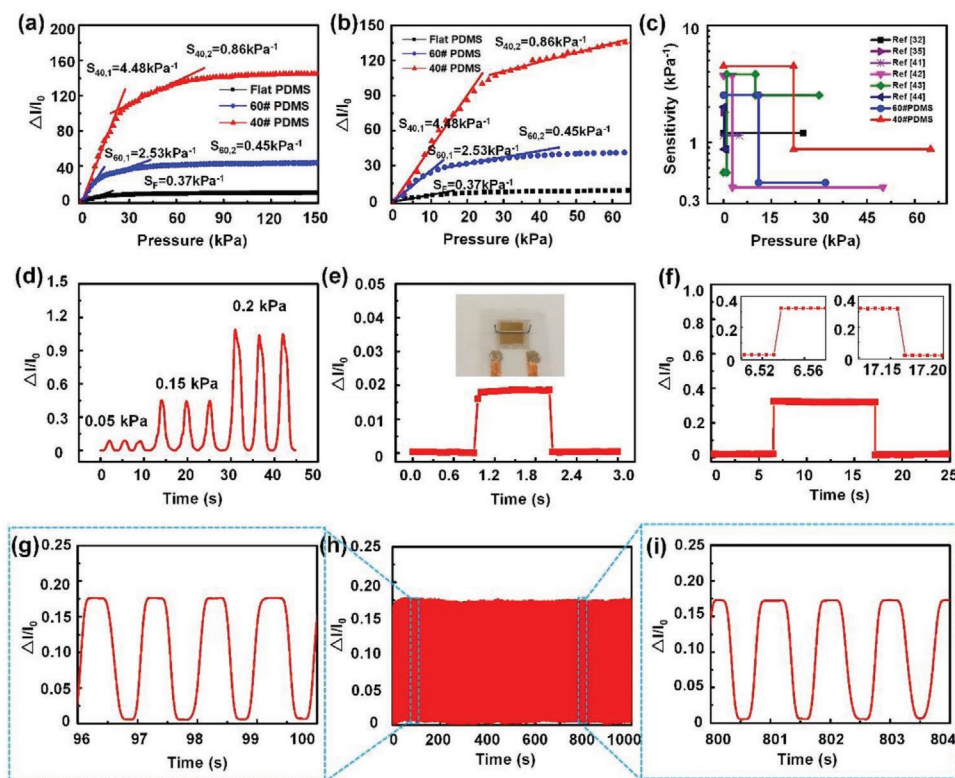
Therefore, hierarchical microstructures can be controllable by adjusting the laser power and scanning spaces (Figure 2a (iii)).

Figure 2d–f show the surface images of laser-scribed PDMS (#40 sample). The surface of #40 sample is constructed of periodical microstructures of a big quadrangular frustum pyramid and two small quadrangular pyramids. The big quadrangular frustum pyramids have a bottom edge of  $40 \mu\text{m}$ , a top edge of  $20 \mu\text{m}$ , and a height of  $20 \mu\text{m}$ . The small quadrangular pyramids have a footprint of  $40 \mu\text{m} \times 20 \mu\text{m}$  and a height of about  $10 \mu\text{m}$  (Figure 2g). Figure 2h–j show the surface images of AgNWs-coated PDMS, where both the upper surface and the sidewalls of the microstructures are uniformly covered with AgNWs. And the profile of the microstructures remains almost the same as shown in Figure 2k. Furthermore, the results for #60 sample are shown in Figure S4, Supporting Information. The surface is constructed of periodical microstructures of a big quad-rangular frustum pyramid (with bottom edges of  $60 \mu\text{m}$ ,

top edges of  $40 \mu\text{m}$ , and heights of  $16 \mu\text{m}$ ) and three small quadrangular pyramids (with footprints of  $60 \mu\text{m} \times 20 \mu\text{m}$  and heights of  $12 \mu\text{m}$ ). Similarly, the profile of #60 sample changes little after uniformly coated with AgNWs.

### 2.3. The Performance of the Flexible Pressure Sensor

The performance of the flexible pressure sensor with hierarchical microstructures is tested by measuring the relative current variations of the interdigital electrode with pressure applied on the PDMS surface. The current variation ratios ( $\Delta I/I_0 = (I - I_0)/I_0$ , where  $I_0$  and  $I$  are the initial current and current under applied pressure) are calculated on the basis of measured values and are plotted as a function of applied pressure as shown in Figure 3a. The pressure sensitivity  $S$  ( $S = \Phi(\Delta I/I_0)/\Phi P$ , where  $P$  is the applied pressure) is defined as the slope of curve in Figure 3b.



**Figure 3.** a,b) The relative current variations  $\Delta I/I_0$  of flat, #40, and #60 PDMS sensors under different pressures. c) Comparison of the sensitivity and pressure range between laser-scribed sensors and previously reported flexible pressure sensors. d) Current response to increased pressures under loading and unloading at 0.05, 0.15, and 0.2 kPa (#40). e) Relative current change under a subtle pressure of 3 Pa. f) The response time and recovery time of the #40 pressure sensor under 0.1 kPa. g–i) The reliability test of the #40 pressure sensor under 0.06 kPa for 1000 cycles (#40).

For the #40 sample, the sensitivity is  $4.48 \text{ kPa}^{-1}$  for 0–22 kPa and  $0.86 \text{ kPa}^{-1}$  for 27–65 kPa. For the #60 sample, the sensitivity is  $2.53 \text{ kPa}^{-1}$  in the range of 0–10 kPa and  $0.45 \text{ kPa}^{-1}$  in the range of 13–35 kPa. Meanwhile, the flat sample shows little response to pressure and the sensitivity is about  $0.37 \text{ kPa}^{-1}$ . This means that the sensitivity of hierarchical micro-structured sensors is at least 10 times higher than that of the flat one. Also, the performance of the sensors is superior to some of previous researches as shown in Figure 3c.<sup>[40,43,48–51]</sup> The mechanism is that the first order microstructures deform dramatically as pressure is loaded, leading to a rapid increase in contact area. The current increases sharply and causes high sensitivity. As the pressure continues to increase, in the first order microstructures, the increase rates of contact area and current are both decreased. But the second order microstructures deform dramatically, and the sensitivity improves effectively. The results show that designed hierarchical microstructures do help improving both the sensitivity as well as the linear measuring range of the flexible pressure sensor. And the profile of the microstructures affects the specific performance. By comparing the results of #60 and #40 samples, it can be concluded that the sensitivity and linear measuring range can be improved simultaneously with proper geometry.

Due to the higher sensitivity and wider pressure range, the #40 sample is used for the following performance test and application presentation. Different pressures of 0.05, 0.15, and 0.2 kPa have been applied on the sensor to test its dynamic response, and the results are shown in Figure 3d. To investigate

the ability for detecting subtle pressure, a staple is put onto the sensor, in which the pressure is estimated as 3 Pa, and the results are shown in Figure 3e. Moreover, a test of loading and unloading of 0.1 kPa is carried out to test the response rate. The corresponding response time for loading and unloading is both less than 7 ms, indicating a real-time response ability (Figure 3f). The flexible pressure sensor is fixed on plastic rods with different diameters ( $D = 10, 18, \text{ and } 25 \text{ mm}$ ). The same staples are used to test the performance of the pressure sensor. The results show that the sensor works normally on the curved surfaces (Figure S5, Supporting Information). To further investigate the stability of the pressure sensor under repeated loading, a fatigue test (with load pressure of 0.06 kPa) is conducted for 1000 cycles, as shown in Figure 3g–i. The output relative current variation shows good durability with no obvious degeneration over 1000 cycles, which is significant for long-term applications.

#### 2.4. Application of the Flexible Pressure Sensor

Endowed with features of flexibility, high sensitivity, and relatively large linear measuring range, the hierarchical micro-structured pressure sensor is extremely suitable for human health monitoring. The waveform of arterial pulsation has been regarded as an indicator for several diseases, for instance, cardiovascular disease or diabetes.<sup>[52]</sup> This pressure sensor is attached to the radial artery of an adult to detect the pulse

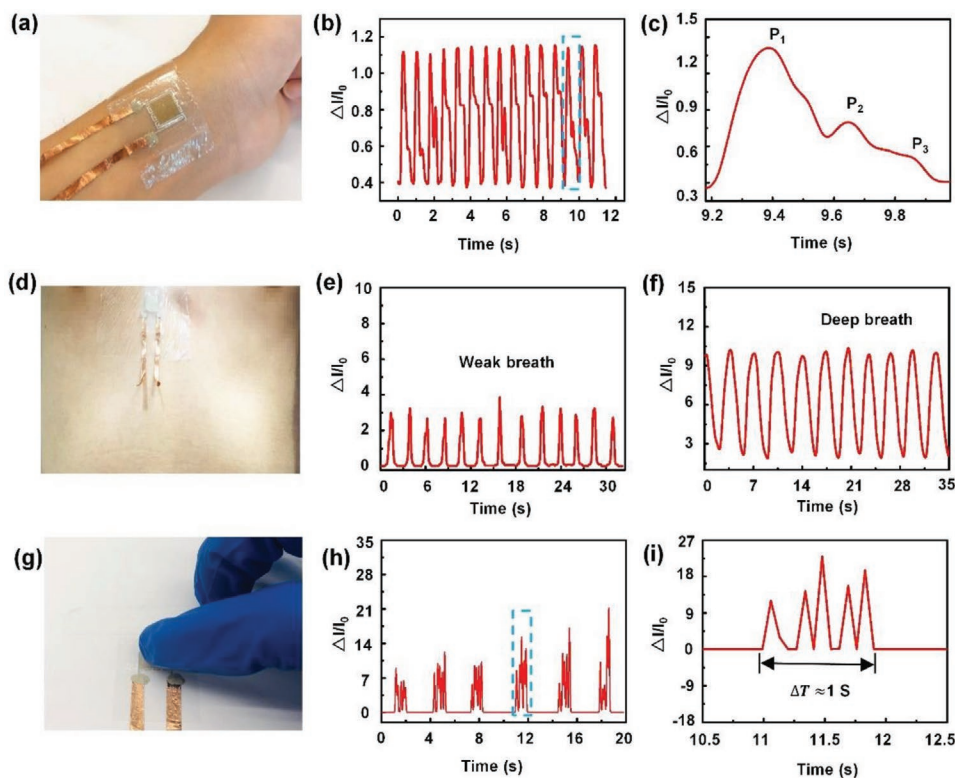


**Figure 4.** a–c) Sensing performance of the pressure sensor coated on the wrist for sensing the wrist pulse. d–f) Photograph of a pressure sensor attached on the human chest area, indicating different signal variations for weak and deep respiration. g–i) Sensing performance of the sensor under imitated knocking of early-stage Parkinson’s disease featuring a static tremor frequency of 5 Hz.

signals, as shown in **Figure 4a**. **Figure 4b** displays the real-time monitoring signals, and the corresponding heart beating rate is about 82 bpm. Three subtle peaks, including  $P_1$  (percussion wave),  $P_2$  (tidal wave), and  $P_3$  (diastolic wave), can be identified clearly in the zoom-in image of a pulse signal (**Figure 4c**). The subtle pulse features can be captured with this highly sensitive device and the large linear range shall enable simpler mathematical models for physiological parameters like blood pressure.

The pressure sensor can be also applied to monitor obstructive sleep apnea syndrome, which is related to human respiration.<sup>[53]</sup> **Figure 4d** shows the pressure sensor attached to the human chest. It shows that the pressure sensor can distinguish the weak breath and deep breath. The weak and deep respiratory rate is 24 and 18 bpm, respectively (**Figure 4e,f**).

In addition, the pressure sensor also has been used to monitor early-stage Parkinson’s disease (PD), which is a kind of neurodegenerative disease and has a feature of static tremulous frequency at 4–6 Hz.<sup>[50]</sup> Knocking the pressure sensor at a relative frequency simulates the PD with static tremors (**Figure 4g**). It is demonstrated that the knocking frequency is about 5 Hz and has potential application in predicating early-stage Parkinson’s disease (**Figure 4h,i**).

What’s more, since laser direct writing and ink-jet printing are typical manufacturing methods for large-area electronics, the proposed strategy to design and fabricate flexible hierarchical microstructured pressure sensors is scalable. To demonstrate the scalability of this strategy, a  $3 \times 3$  array sensor

has been fabricated all by laser direct writing, as shown in **Figure 5a**. The array sensor is composed of two functional layers and an encapsulation layer. The AgNWs coating on the micro-structured PDMS is patterned into a chessboard by laser with relatively smaller power, and each box represents a sensing point. And the interdigital electrodes are made from ITO/PET film, which is patterned by laser writing. The final product is shown in the bottom right of **Figure 5a**, and the device can be conformal on the glass cylinder ( $R = 10$  mm). Chinese coin and staples are used to test the performance of the array device. The results are shown in **Figure 5b**, and it indicates that the array device is working normally on the curved surface. Therefore, this strategy is highly promising to enable intelligent robotics or other equipment with smart sensing.

### 3. Conclusions

In summary, we have presented a facile and scalable strategy to fabricate flexible pressure sensors with hierarchical microstructures. The laser-ablated hierarchical microstructures have induced a high sensitivity of  $4.48 \text{ kPa}^{-1}$  in the linearity range from 0 to 22 kPa and  $0.86 \text{ kPa}^{-1}$  in the linearity range from 27 to 65 kPa, a low detection ability of 3 Pa, fast response time less than 7 ms, and excellent reliability for over 1000 cycles. The flexible pressure sensor can be used for monitoring wrist pulse, breathing, and static tremors. In addition, a flexible pressure sensor array is further fabricated and can map the spatial

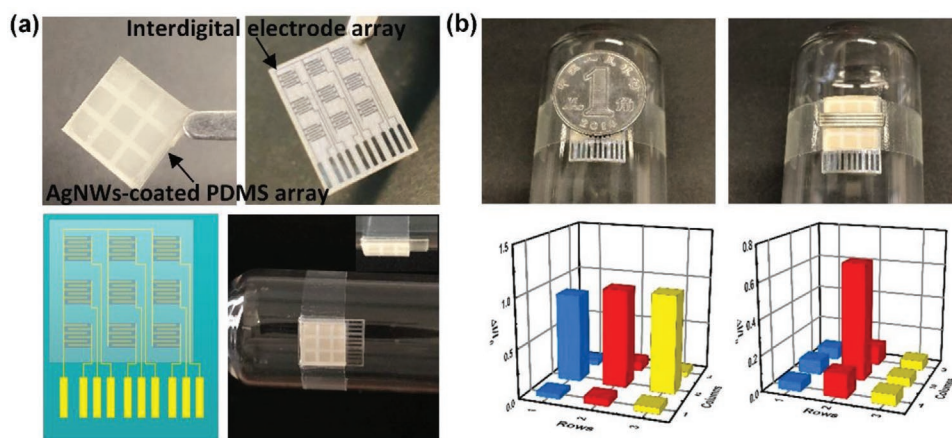


**Figure 5.** a) Laser-scribed microstructure array on PDMS surface, interdigital electrode array on ITO/PET surface, and the flexible pressure sensor array fixed on the wall of a test tube. b) A coin and staples positioned over the flexible pressure sensor array fixed on the wall of a test tube, and the corresponding response mapping of the pressure distribution.

pressure distribution well. The simple and scalable fabrication process and high-performance of the flexible pressure sensor indicate its potential applications in wearable medical monitoring devices and human-machine interface.

## 4. Experimental Section

**Preparation of the Microstructured Polydimethylsiloxane:** The PDMS precursor and curing agent (Sylgard 184, Dow Corning) was mixed with a weight ratio of 10:1. The PDMS mixture was poured into a square PMMA mold and air bubbles were removed in a vacuum drying oven. After 3 h heating at 80 °C, the flat PDMS film with a thickness of 1 mm was obtained. Then a commercial femtosecond laser (Workshop of Photonics, wavelength: 355 nm, Maximal repetition rate: 1 MHz, pulse width: 500 fs) was used to ablate hierarchical microstructures on the PDMS film.

Different heights of microstructures were obtained by adjusting laser scanning spaces. Two kinds of grid pattern were scribed by laser scanning path, in which the spacing between the two adjacent lines was 40 and 60  $\mu\text{m}$ , respectively. Then, the spacing of lines was alternately filled with 20  $\mu\text{m}$  interval lines. The laser power was about 1 W and the scanning speed was about 800  $\text{mm s}^{-1}$ . Finally, the laser-scribed PDMS was cut into small pieces (10 mm  $\times$  10 mm), cleaned with ethanol and dried for the next step.

**Preparation of the Silver Nanowires Film:** Ultrathin AgNWs were synthesized as described in the literature.<sup>[54]</sup> 2 g polyvinylpyrrolidone (PVP) was dissolved in 100 mL ethylene glycol (EG). 1 mL of tetrabutylammonium chloride was added to the PVP solution. 50 mL  $\text{AgNO}_3$  solution (0.2 M) was added into the mixture and stirred for 2 h at 160 °C. The reaction product was washed with deionized water three times and centrifuged to remove the extra chemical agents. The AgNWs were re-dispersed in 10 mL deionized water with 10  $\text{mg mL}^{-1}$  concentration, and 1 mg polyvinyl alcohol was added into the solution to improve the adhesion between AgNWs and microstructured PDMS. The surface of micro-structured PDMS was pretreated with oxygen plasma and spin-coated with AgNWs solution at 2000 rpm for 20 s. The AgNWs/PDMS film was obtained after placing it on the hot plate at 80 °C for 30 min.

**Fabrication of the Flexible Pressure Sensor:** Interdigital electrode was printed on a PET film using a Nordson EFD printer (PRO4L/A). The film was pretreated 1 min with oxygen plasma. Different interdigital electrodes were printed with a printing speed of 50  $\text{mm s}^{-1}$ . After printing, the PET films were dried at 80 °C for 30 min. The flexible pressure sensor was assembled with AgNWs/PDMS film and interdigital electrode on PET followed by encapsulating with surgical semipermeable polyurethane film (Bengbu Chongdi Biotechnology Co., LTD).

**Fabrication of the Flexible Pressure Sensor Array:** The pressure sensor array was fabricated by scaling up the interdigital electrode into a 3  $\times$  3 array. The PDMS elastomer was spin-coated with a layer of AgNWs film, and then the conductive AgNWs layer was divided into 3  $\times$  3 pixels by laser ablation. The area of each pixel was 2.5 mm  $\times$  2.5 mm, and the distance between two pixels was 0.75 mm. The interdigital electrode array was fabricated by laser ablation of ITO/PET film. The width of the interdigital electrode was 0.2 mm and the spacing between two adjacent electrodes was also 0.2 mm.

**Performance Measurements and Characterization:** To investigate the performance of the flexible pressure sensor, compression tests were conducted by a situ biaxial fatigue testing system (IPBF-300L, China). The resistance signals were recorded by a digital multimeter (Keysight 34 461 A, USA). 3D morphology of the microstructured PDMS was analyzed by digital microscope (VHX-6000, Japan). The micro-morphology and microstructure of the PDMS samples were analyzed by a field emission scanning electron microscope (S-4800) at acceleration voltage of 10 kV.

## Supporting Information

Supporting Information is available from the Wiley Online Library or from the author.

## Acknowledgements

This work was supported by National Natural Science Foundation of China (Grant No. 11625207, U20A6001, 11902292), the Zhejiang Province Key Research and Development Project (Grant No. 2019C05002, 2020C05004, 2021C01183), and Natural Science Foundation of Zhejiang Province (Grant No. LQ20E030008, LQ20E050014, LQ19E030003).

## Conflict of Interest

The authors declare no conflict of interest.

## Data Availability Statement

The data that support the findings of this study are available from the corresponding author upon reasonable request.

## Keywords

flexible electronics, hierarchical microstructure, laser processing, pressure sensor, wearable biomedical device

Received: February 1, 2021

Revised: April 23, 2021

Published online:

- [1] J. C. Yang, J. Mun, S. Y. Kwon, S. Park, Z. Bao, S. Park, *Adv. Mater.* **2019**, *31*, 1904765.
- [2] Z. Lou, S. Chen, L. Wang, K. Jiang, G. Shen, *Nano Energy* **2016**, *23*, 7.
- [3] S. K. Ameri, R. Ho, H. Jang, L. Tao, Y. Wang, L. Wang, D. M. Schnyer, D. Akinwande, N. Lu, *ACS Nano* **2017**, *11*, 7634.
- [4] S. J. Park, J. Kim, M. Chu, M. Khine, *Adv. Mater. Technol.* **2018**, *3*, 1700158.
- [5] Y. Cai, J. Shen, Z. Dai, X. Zang, Q. Dong, G. Guan, L. J. Li, W. Huang, X. Dong, *Adv. Mater.* **2017**, *29*, 1606411.
- [6] L. Li, L. Pan, Z. Ma, K. Yan, W. Cheng, Y. Shi, G. Yu, *Nano Lett.* **2018**, *18*, 3322.
- [7] S. Jung, J. H. Kim, J. Kim, S. Choi, J. Lee, I. Park, T. Hyeon, D. H. Kim, *Adv. Mater.* **2014**, *26*, 4825.
- [8] T. Chang, Y. Tian, C. Li, X. Gu, K. Li, H. Yang, P. Sanghani, C. M. Lim, H. Ren, P. Chen, *ACS Appl. Mater. Interfaces* **2019**, *11*, 10226.
- [9] G. Schwartz, B. C. Tee, J. Mei, A. L. Appleton, D. H. Kim, H. Wang, Z. Bao, *Nat. Commun.* **2013**, *4*, 1859.
- [10] M. J. Cima, *Nat. Biotechnol.* **2014**, *32*, 642.
- [11] K. Shin, J. S. Lee, J. Jang, *Nano Energy* **2016**, *22*, 95.
- [12] Z. Chen, Z. Wang, X. Li, Y. Lin, N. Luo, M. Long, N. Zhao, J. Xu, *ACS Nano* **2017**, *11*, 4507.
- [13] Y. Yang, J. J. Qi, Y. S. Gu, X. Q. Wang, Y. Zhang, *Phys. Status Solidi RRL* **2009**, *3*, 269.
- [14] Y. S. Zhou, R. Hinchet, Y. Yang, G. Ardila, R. Songmuang, F. Zhang, Y. Zhang, W. Han, K. Pradel, L. Montès, *Adv. Mater.* **2013**, *25*, 883.
- [15] C. M. Boutry, A. Nguyen, Q. O. Lawal, A. Chortos, S. R. Gagné, Z. Bao, *Adv. Mater.* **2015**, *27*, 6954.
- [16] D. Kwon, T. Lee, J. Shim, S. Ryu, M. S. Kim, S. Kim, T. Kim, I. Park, *ACS Appl. Mater. Interfaces* **2016**, *8*, 16922.
- [17] Y. Yang, W. Guo, J. Qi, Y. Zhang, *Appl. Phys. Lett.* **2010**, *97*, 223107.
- [18] Y. Wang, Y. Wang, Y. Yang, *Adv. Energy Mater.* **2018**, *8*, 1800961.
- [19] Z. Han, Z. Cheng, Y. Chen, B. Li, Z. Liang, H. Li, Y. Ma, X. Feng, *Nanoscale* **2019**, *11*, 5942.
- [20] A. Tewari, S. Gandla, S. Bohm, C. R. McNeill, D. Gupta, *ACS Appl. Mater. Interfaces* **2018**, *10*, 5185.
- [21] J. Zou, M. Zhang, J. Huang, J. Bian, Y. Jie, M. Willander, X. Cao, N. Wang, Z. L. Wang, *Adv. Energy Mater.* **2018**, *8*, 1702671.
- [22] Y. C. Lai, J. Deng, R. Liu, Y. C. Hsiao, S. L. Zhang, W. Peng, H. M. Wu, X. Wang, Z. L. Wang, *Adv. Mater.* **2018**, *30*, 1801114.
- [23] K. Zhao, Z. L. Wang, Y. Yang, *ACS Nano* **2016**, *10*, 9044.
- [24] H. Wang, Z. Xiang, P. Giorgia, X. Mu, Y. Yang, Z. L. Wang, C. Lee, *Nano Energy* **2016**, *23*, 80.
- [25] X. Zhao, B. Chen, G. Wei, J. M. Wu, W. Han, Y. Yang, *Adv. Mater. Technol.* **2019**, *4*, 1800723.
- [26] Y. Wang, H. Wu, L. Xu, H. Zhang, Y. Yang, Z. L. Wang, *Sci. Adv.* **2020**, *6*, eabb9083.
- [27] W. Chen, X. Gui, B. Liang, R. Yang, Y. Zheng, C. Zhao, X. Li, H. Zhu, Z. Tang, *ACS Appl. Mater. Interfaces* **2017**, *9*, 24111.
- [28] Z. Huang, M. Gao, Z. Yan, T. Pan, S. A. Khan, Y. Zhang, H. Zhang, Y. Lin, *Sens. Actuators, A* **2017**, *266*, 345.
- [29] D. Lee, H. Lee, Y. Jeong, Y. Ahn, G. Nam, Y. Lee, *Adv. Mater.* **2016**, *28*, 9364.
- [30] Y. Wei, S. Chen, X. Dong, Y. Lin, L. Liu, *Carbon* **2017**, *113*, 395.
- [31] L. Pan, A. Chortos, G. Yu, Y. Wang, S. Isaacson, R. Allen, Y. Shi, R. Dauskardt, Z. Bao, *Nat. Commun.* **2014**, *5*, 3002.
- [32] C. L. Choong, M. B. Shim, B. S. Lee, S. Jeon, D. S. Ko, T. H. Kang, J. Bae, S. H. Lee, K. E. Byun, J. Im, *Adv. Mater.* **2014**, *26*, 3451.
- [33] Y. Lee, J. Park, S. Cho, Y. Shin, H. Lee, J. Kim, J. Myoung, S. Cho, S. Kang, C. Baig, *ACS Nano* **2018**, *12*, 4045.
- [34] Y. Mao, B. Ji, G. Chen, C. Hao, B. Zhou, Y. Tian, *ACS Appl. Nano Mater.* **2019**, *2*, 3196.
- [35] P. Nie, R. Wang, X. Xu, Y. Cheng, X. Wang, L. Shi, J. Sun, *ACS Appl. Mater. Interfaces* **2017**, *9*, 14911.
- [36] Q. Shao, Z. Niu, M. Hirtz, L. Jiang, Y. Liu, Z. Wang, X. Chen, *Small* **2014**, *10*, 1466.
- [37] B. Zhu, Z. Niu, H. Wang, W. R. Leow, H. Wang, Y. Li, L. Zheng, J. Wei, F. Huo, X. Chen, *Small* **2014**, *10*, 3625.
- [38] Y. Zhang, Y. Hu, P. Zhu, F. Han, Y. Zhu, R. Sun, C. Wong, *ACS Appl. Mater. Interfaces* **2017**, *9*, 35968.
- [39] M. Jian, K. Xia, Q. Wang, Z. Yin, H. Wang, C. Wang, H. Xie, M. Zhang, Y. Zhang, *Adv. Funct. Mater.* **2017**, *27*, 1606066.
- [40] X. Wang, Y. Gu, Z. Xiong, Z. Cui, T. Zhang, *Adv. Mater.* **2014**, *26*, 1336.
- [41] B. Su, S. Gong, Z. Ma, L. W. Yap, W. Cheng, *Small* **2015**, *11*, 1886.
- [42] X. Tang, C. Wu, L. Gan, T. Zhang, T. Zhou, J. Huang, H. Wang, C. Xie, D. Zeng, *Small* **2019**, *15*, 1804559.
- [43] J. Shi, L. Wang, Z. Dai, L. Zhao, M. Du, H. Li, Y. Fang, *Small* **2018**, *14*, 1800819.
- [44] C. Lu, Y. Gao, G. Yu, M. Xu, J. Tan, F. Xuan, *Sens. Actuators, A* **2018**, *281*, 124.
- [45] Y. Zhu, H. Cai, H. Ding, N. Pan, X. Wang, *ACS Appl. Mater. Interfaces* **2019**, *11*, 6195.
- [46] P. Gordon, B. Balogh, B. Sinkovics, *Microelectron. Reliab.* **2007**, *47*, 347.
- [47] H. W. Choi, S. Bong, D. F. Farson, C. Lu, L. J. Lee, *J. Laser Appl.* **2009**, *21*, 196.
- [48] S. Gong, W. Schwalb, Y. Wang, Y. Chen, Y. Tang, J. Si, B. Shirinzadeh, W. A. Cheng, *Nat. Commun.* **2014**, *5*, 3132.
- [49] M. J. Yin, Y. Zhang, Z. Yin, Q. Zheng, A. P. Zhang, *Adv. Mater. Technol.* **2018**, *3*, 1800051.
- [50] Y. Guo, M. Zhong, Z. Fang, P. Wan, G. Yu, *Nano Lett.* **2019**, *19*, 1143.
- [51] H. Park, Y. R. Jeong, J. Yun, S. Y. Hong, S. Jin, S. Lee, G. Zi, J. S. Ha, *ACS Nano* **2015**, *9*, 9974.
- [52] P. Wei, X. Guo, X. Qiu, D. Yu, *Nanotechnology* **2019**, *30*, 455501.
- [53] Y. Pang, K. Zhang, Z. Yang, S. Jiang, Z. Ju, Y. Li, X. Wang, D. Wang, M. Jian, Y. Zhang, *ACS Nano* **2018**, *12*, 2346.
- [54] J. Lu, D. Liu, J. Dai, *J. Mater. Sci.: Mater. Electron.* **2019**, *30*, 15786.